



Influence of Iliac Stenotic Lesions on Blood Flow Patterns Near a Covered Endovascular Reconstruction of the Aortic Bifurcation (CERAB) Stent Configuration

Journal of Endovascular Therapy
 2017, Vol. 24(6) 800–808
 © The Author(s) 2017
 Reprints and permissions:
sagepub.com/journalsPermissions.nav
 DOI: 10.1177/1526602817732952
www.jevt.org
 

Erik Groot Jebbink, MSc^{1,2,3}, Stefan Engelhard, MSc^{1,2}, Guillaume Lajoinie, PhD^{2,3}, Jean-Paul P. M. de Vries, MD, PhD⁴, Michel Versluis, PhD^{2,3}, and Michel M. P.J. Reijnen, MD, PhD¹

Abstract

Purpose: To investigate the effect of distal stenotic lesions on flow patterns near a covered endovascular reconstruction of the aortic bifurcation (CERAB) configuration used in the treatment of aortoiliac occlusive disease. **Method:** Laser particle image velocimetry measurements were performed using in vitro models of the aortic bifurcation with and without a CERAB configuration in place. A hemodynamically nonsignificant stenosis (ΔP : 9 mm Hg), a hemodynamically significant (ΔP : 26 mm Hg) stenosis, and a total occlusion were simulated in the left iliac arteries. Velocity fields and time-averaged wall shear stress (TAWSS) were calculated. **Results:** Hemodynamically significant distal lesions did not influence the inflow patterns or TAWSS (0.5–0.6 Pa) in either model. However, hemodynamically significant distal stenotic lesions caused a 2-fold decrease in peak outflow velocities (control: 106 vs 56 cm/s, CERAB: 96 vs 54 cm/s) and a 3-fold decrease in TAWSS (control: 1.34 vs 0.44 Pa, CERAB: 0.75 vs 0.21 Pa). There was a 2-fold decrease in wall shear stress in the CERAB outflow compared with the control, independent of lesion severity. **Conclusion:** In the CERAB technique, adequate distal runoff is identified as an important parameter to ensure patency. This in vitro study showed that distal stenotic lesions influence aortic bifurcation outflow patterns and TAWSS more extensively in the CERAB configuration. Distal stenotic lesions could therefore increase the risk of disease progression and loss of stent patency. In vivo studies are necessary to confirm these observations.

Keywords

aorta, aortic bifurcation, aortoiliac occlusive disease, in vitro experiment, flow model, neobifurcation, occlusion, particle image velocimetry, runoff, stenosis, stent

Introduction

Traditionally, the treatment of choice for extensive aortoiliac occlusive disease has been open surgery, while the kissing stents technique has been applied in the last decades for less complex lesions. A recent alternative therapy for extensive disease is the covered endovascular reconstruction of the aortic bifurcation (CERAB) technique.¹ Satisfying early results have been reported, with primary and secondary patency rates of 87% and 95%, respectively, at 2 years' follow-up in a group with >80% TransAtlantic Inter-Society Consensus II D lesions.¹ This patient selection makes it difficult to compare the results to studies of other endovascular techniques that have included fewer type D lesions.

In an in vitro setup, our group recently showed that regional flow patterns around the CERAB configuration

are more comparable to physiologic flow than those in bare metal or covered kissing stents.² Pathophysiologic wall shear stress (WSS) at the in- and outflow of the configurations are also of interest as WSS may promote the

¹Department of Vascular Surgery, Rijnstate Hospital, Arnhem, the Netherlands

²MIRA Institute for Biomedical Technology and Technical Medicine, University of Twente, Enschede, the Netherlands

³Physics of Fluids Group, Faculty of Science and Technology, University of Twente, Enschede, the Netherlands

⁴Department of Vascular Surgery, St Antonius Hospital, Nieuwegein, the Netherlands

Corresponding Author:

Erik Groot Jebbink, Department of Surgery, Rijnstate Hospital, Wagnerlaan 55, 6815 AD Arnhem, the Netherlands.
 Email: erik.grootjebbink@gmail.com

development of atherosclerotic plaque and, in turn, could affect stent patency due to the occurrence of restenosis.³ However, it is still unclear how these flow patterns and WSS values are influenced by stenotic lesions in the iliac artery distal to the stent configuration. These lesions may cause poor runoff, which has been identified as a risk factor for stent failure.⁴⁻⁷ A previous study evaluating the CERAB technique also suggested that outflow obstructions distal to a CERAB reconstruction could reduce primary patency.¹ Therefore, this study investigated the influence of distal stenotic lesions on blood flow patterns and quantified WSS values near the CERAB configuration.

Methods

Model Design and Experimental Setup

Laser particle image velocimetry (PIV) measurements were performed to obtain velocity vector fields of a rigid in vitro silicone model of the abdominal aorta with renal arteries, common iliac arteries (CIA), and a CERAB configuration in place. The CERAB configuration (Figure 1) was constructed in-house using a platform based on the fully covered Advanta V12 stents (Atrium Maquet Getinge Group, Mijdrecht, the Netherlands).² Two 8-mm Atrium V12 stents (the limbs) were placed within the distal part of a funnel-shaped, large-diameter, tapered V12 stent (16 mm proximally tapering to 12 mm distally). The neobifurcation started ~20 mm proximal to the anatomic bifurcation (Figure 1). The white polytetrafluoroethylene covers were replaced by transparent polyurethane to obtain optical access. To simulate stenoses for some of the experiments, 1-cm-long inserts with reduced diameters were placed in the 8-mm outflow tube representing the left CIA. Measurements performed in the CERAB model were compared to a control model without stents.

The flow models and experimental setup were previously described^{2,8,9} and are shown in Figure 2. Systolic and diastolic blood pressures were set to 130 and 90 mm Hg, respectively. A heart rate of 60 beats per minute and a mean 1.6-L/min suprarenal inflow, divided equally over both renal and both iliac vessels, created physiologic pulsatile flow conditions (Figure 3).¹⁰

Light from a continuous wave 532-nm laser (Cohlibri; LIGHTLINE lasertechnik GmbH, Osnabrück, Germany) was transformed into a laser sheet (40-mm width, <1-mm thickness) using cylindrical lenses. The laser sheet illuminated the central plane of the model. A high-speed camera (Fastcam SA-X2; Photron Inc, Tokyo, Japan) captured the fluorescence from the 1- to 20- μ m tracer particles (Dantec Dynamics A/S, Skovlunde, Denmark) during 12 heartbeats at 1000 frames per second (fps) at the inflow and at 2000 fps at the outflow of the CERAB configuration (the outflow contained higher peak velocity values, requiring a higher frame rate). The frame rate was chosen to maximize the

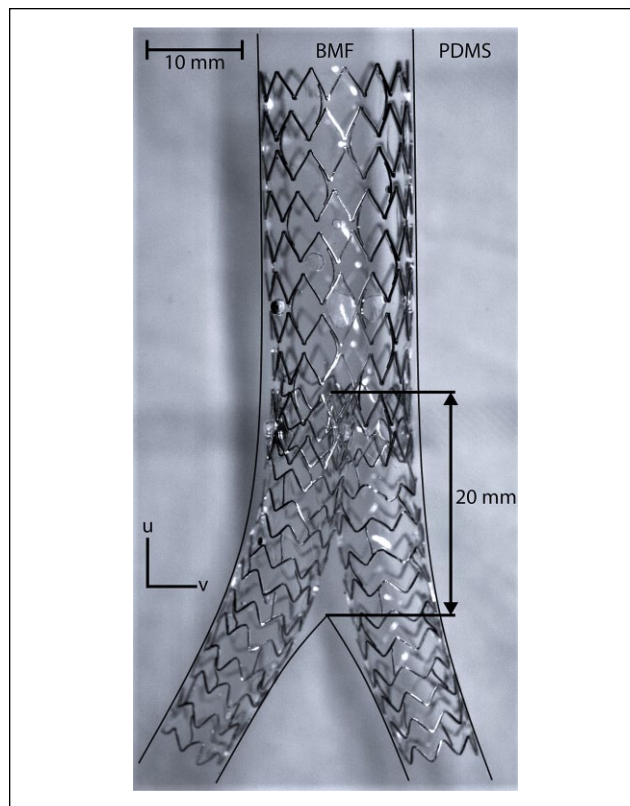


Figure 1. Covered endovascular reconstruction of the aortic bifurcation (CERAB) using Atrium V12 stents placed in an in vitro infrarenal aorta model filled with blood mimicking fluid (BMF). The white polytetrafluoroethylene covers were replaced by transparent polyurethane to obtain optical access. The black lines indicate the vessel walls, which are otherwise invisible due to refractive index matching between the silicone vessel phantom and the BMF. *u* and *v* represent the direction components of the velocity vector. The 2-headed arrow indicates the distance between the anatomic bifurcation and the neobifurcation. PDMS, polydimethylsiloxane.

correlation peaks of particle displacement with respect to the observed velocities of the region of interest (ROI). A long-pass filter, with a cutoff wavelength of 625 nm, was used to filter out reflecting laser light at 532 nm.

Measurements

Images were captured in 2 ROIs at the inflow (distal aorta) and outflow (left CIA), depicted as positions 1 and 2 in Figure 2. Four measurements were performed in each ROI using modified iliac outflow conditions (a healthy distal artery, a hemodynamically nonsignificant stenosis, a hemodynamically significant stenosis, and a total occlusion) in both the control and CERAB models (Table 1). Total occlusion was simulated by clamping the vessel only for the inflow ROI measurements because during total occlusion

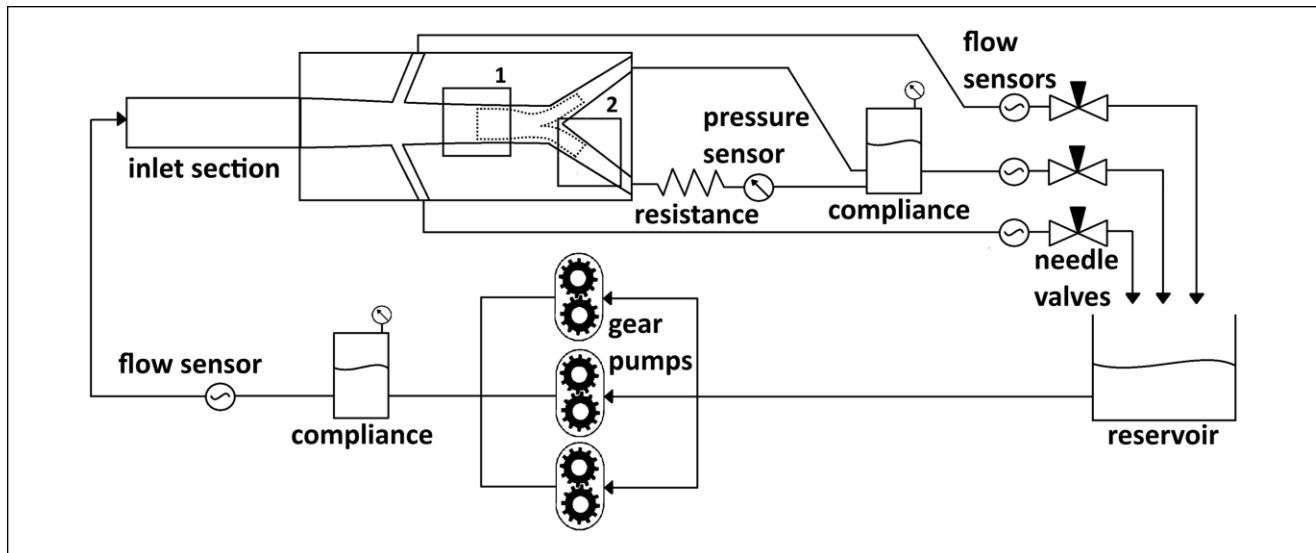


Figure 2. Schematic representation of the experimental setup, where 1 is the inflow region of interest (ROI) and 2 is the outflow ROI. The dashed lines indicate the contours of the covered endovascular reconstruction of the aortic bifurcation (CERAB) deployed in the vessel phantom. The setup was based on a second-order Windkessel model. The inlet section (~100 cm) ensured fully developed flow entering the model. Peripheral resistance was controlled with needle valves. The compliance distal to the vessel phantom was used to model the peripheral dispensability of the vessels. The circulating blood mimicking fluid was a mixture of water (47.4%), glycerol (36.9%), and sodium iodide (15.7%). The resistance was added to mimic an outflow stenosis.

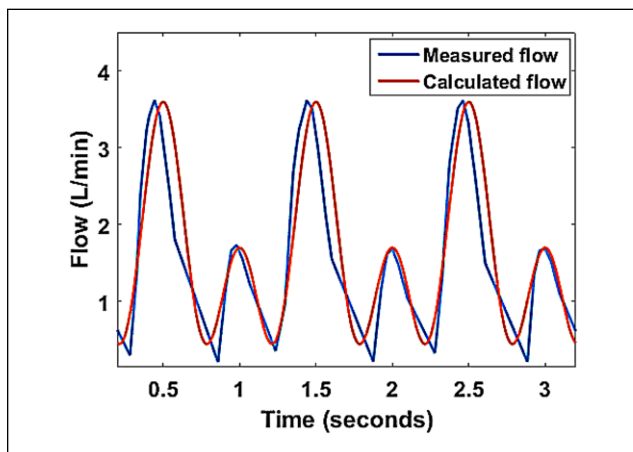


Figure 3. Suprarrenal flow pattern used as input for the model. The flow profile that was used to control the gear pumps is in red and the measured flow at the inlet section of the setup is in blue.

no flow and consequently no shearing force were present in the left CIA.

Pressure gradients across the stenotic lesions were measured with a built-in pressure sensor (40PC015G1A; Honeywell International Inc, Morris Plains, NJ, USA) distal to the stenosis location. Systolic pressure at the bifurcation was used to calculate the pressure difference. The obtained pressure gradients across the stenotic lesions corresponded with physiologic observations.^{11,12} The experiments were

run twice using the same setups and conditions; the results of each sample location were averaged.

Data Analysis

Pre- and postprocessing was performed using MATLAB (The Math Works Inc, Natick, MA, USA).² PIV analysis was performed through pairwise cross-correlation in all captured images using the PIVlab tool (version 1.4) for MATLAB. Velocity vector fields during peak systolic velocity (PSV) and end-systolic velocity (ESV) were obtained.

WSS was calculated as $\mu(\delta u / \delta y)$ where u is the velocity along the vessel wall, y is the height above the vessel wall, $\delta u / \delta y$ is the flow gradient perpendicular to the vessel wall, and μ is the dynamic viscosity of the blood mimicking fluid (BMF; Figure 1). WSS analysis was performed for the wall segments captured in each ROI through interpolation of the velocity data at multiple normal vectors, perpendicular to the vessel wall using the no-slip boundary condition for viscous fluids. Time-averaged WSS (TAWSS) was plotted against vessel length; TAWSS values are shown for the left aortic wall in the inflow ROI and the lateral iliac wall in the outflow ROI. Similar TAWSS values were found at the opposite vessel walls. WSS analysis was less accurate inside the CERAB configuration (and not relevant in this study) and was therefore not evaluated.

Table 1. Measurements Obtained for Regions of Interest in Both Models.

Measurement	Control	CERAB	Lumen Diameter, mm	Lumen Loss, %	Pressure Difference, mm Hg
1	No stenosis	No stenosis	8	0	—
2	Insignificant stenosis	Insignificant stenosis	5	38	9
3	Significant stenosis	Significant stenosis	3	63	26
4	Occlusion	Occlusion	0	100	—

Abbreviation: CERAB, covered endovascular reconstruction of the aortic bifurcation.

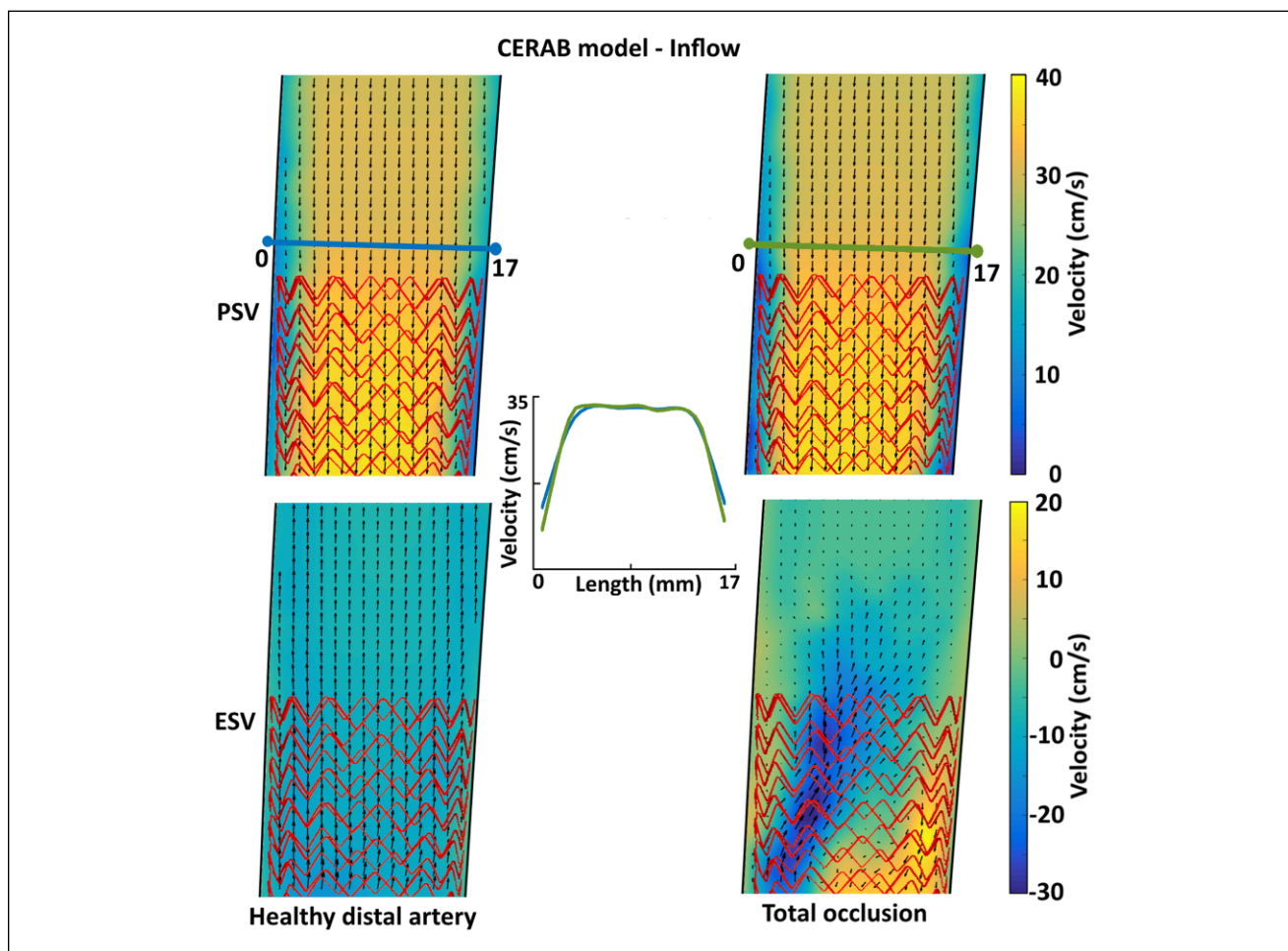


Figure 4. Flow velocity vector fields at the inflow of the covered endovascular reconstruction of the aortic bifurcation (CERAB) model with a healthy distal artery (left) and total occlusion (right) during peak systolic velocity (PSV; upper) and end-diastolic velocity (ESV; lower). Stent mesh indicated in red. The center graph shows axial velocity profiles for both the healthy distal artery and total occlusion situation in the CERAB model during PSV.

Results

Inflow ROI

Similar undisturbed flow patterns were seen in the inflow ROI of the control model and CERAB model with a healthy distal artery during both PSV and EDV. During ESV, backflow velocities near the vessel walls were higher compared

to the velocities in the center of the vessel lumen in both models (Figure 4, bottom).

The flow pattern in the inflow ROI of the control model was not influenced by distal stenosis or occlusion. In the CERAB model, a total occlusion of the distal artery caused an asymmetric flow during ESV but not during PSV (Figure 4, right). During ESV, backflow from the unaffected CIA

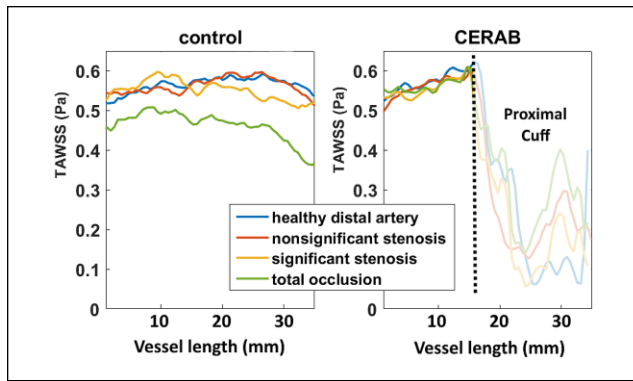


Figure 5. Time-averaged wall shear stress (TAWSS) at the left aortic vessel wall in the inflow region of interest (ROI) of the control and covered endovascular reconstruction of the aortic bifurcation (CERAB) model. The dashed line represents the proximal edge of the CERAB cuff.

was jetted into the proximal CERAB cuff; concurrent recirculation was observed.

In both models, distal stenosis (both nonsignificant and significant) did not influence TAWSS (Figure 5). In the control model, a 20% decrease in TAWSS was observed in a total occlusion of the left CIA. This was not seen in the CERAB configuration (Figure 5).

Outflow ROI

In the setup with healthy distal arteries, flow velocity during PSV in the proximal part of the outflow ROI was 40% lower in the control model than in the CERAB model (57 vs 95 cm/s). In the distal part of the ROI, similar peak flow velocities were seen in the control model and the CERAB model (Figure 6). In the outflow ROI, a more developed, parabolic axial flow profile was present in the CERAB model compared with control, with lower flow velocities near the vessel wall (Figure 7), which caused a smaller velocity gradient with regard to the control.

In both the CERAB and control models, a decrease in velocity during PSV was seen across the vessel lumen with increasing stenosis severity (Figure 7). The nonsignificant stenosis caused a small drop in PSV, while a significant stenosis caused 53% and 56% decreases in the 2 experiment runs (control: 106 vs 56 cm/s, CERAB: 96 vs 54 cm/s).

In the control model, an earlier onset of backflow or flow reversal (FR) was seen with increased stenosis severity (FR in Figure 8). The second moment of FR (back to forward flow) remained the same, indicating that distal stenosis caused a longer duration of backflow. This effect was not observed in the CERAB model.

In both the stented and control models, TAWSS in the outflow ROI decreased due to distal stenosis (Figure 9). In the models with a significant stenosis, there was a 3-fold

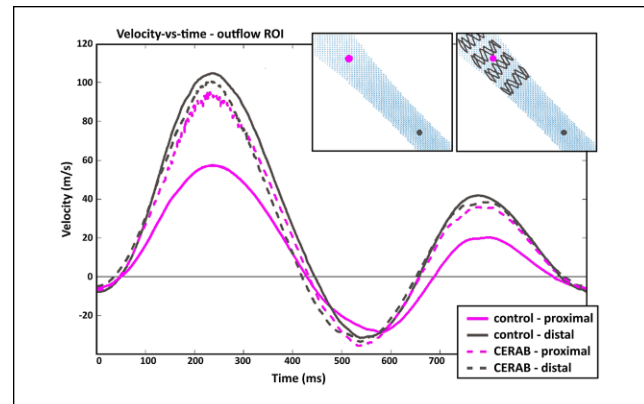


Figure 6. Velocity vs time plot of outflow region of interest (ROI) in the control and covered endovascular reconstruction of the aortic bifurcation (CERAB) model. Locations of velocities are indicated by the gray and purple dots in the top right panels.

decrease in TAWSS compared to the models with healthy distal arteries (average 2–4 cm; control: 0.44 vs 1.34 Pa, CERAB: 0.21 vs 0.75 Pa). In the CERAB model, TAWSS was 2 times lower than in the control model, independent of stenosis severity (average 2–4 cm; healthy: 0.75 vs 1.34 Pa, significant stenosis: 0.21 vs 0.44 Pa).

Discussion

This study has shown that the inflow section of the CERAB and control models are not influenced by outflow stenosis, but an occlusion causes jetting from the nonoccluded limb into the cuff of the CERAB, and a 20% decrease in TAWSS occurs in the control model. In the inflow ROI, the highest velocities during ESV were found near the vessel wall. This was caused by backward flow from the distal aorta toward the renal arteries during ESV. Holenstein and colleagues¹³ attributed the occurrence of backflow to differences in resistance between the renal system and peripheral system of the legs. Velocities near the vessel wall also returned to a forward direction earlier than in the center of the vessel, indicating the presence of a Womersley velocity profile.¹⁴ These phenomena are also known to occur in vivo, which confirms the similarity between the flow conditions in human physiology and the models used in the study.

A 40% decrease in flow velocity measurements during PSV was observed in the control model at the anatomic bifurcation vs the same location in the CERAB model. This can be explained by the fact that the CERAB limbs keep the flow lumen at 8 mm starting at the neobifurcation, whereas the native bifurcation widens before it narrows into the CIA (branch to trunk ratio >1). This influences the observed flow profiles and TAWSS values in the distal iliac vessels.

The observed flow profile in the control model was more blunt or plug-shaped, while in the CERAB the profile was

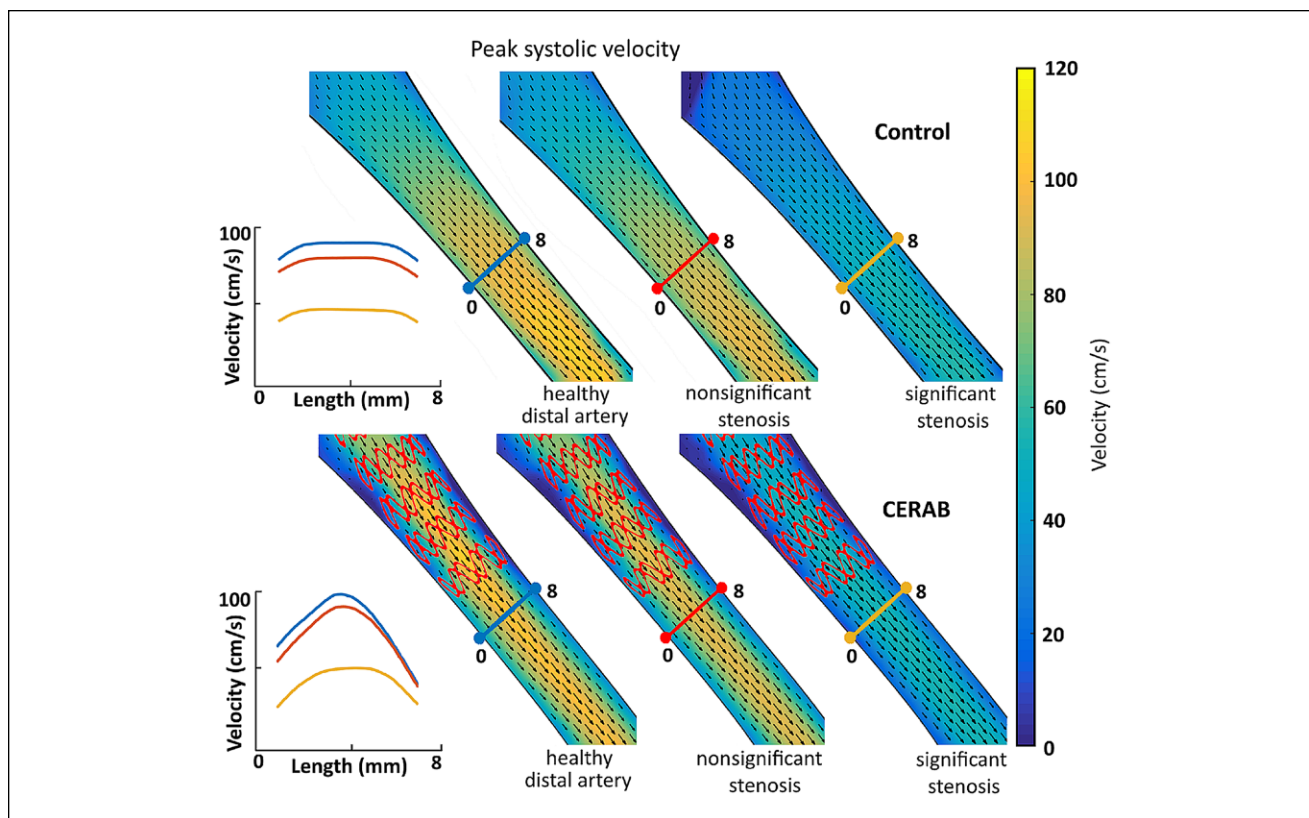


Figure 7. Flow velocity vector fields of the outflow region of interest in the control (upper) and covered endovascular reconstruction of the aortic bifurcation (CERAB; lower) models during peak systolic velocity (PSV). The graphs show axial velocity profiles for the 3 stages of distal outflow stenosis in both the control (upper) and CERAB (lower) model during PSV.

more parabolic, causing a smaller velocity gradient and resulting in lower TAWSS values. This can be attributed to the fact that the outflow profile of the CERAB can develop (ie, become more parabolic) over a longer distance (~20 mm) compared with the control. Therefore, prior to the introduction of a distal stenosis, the TAWSS near the CERAB outflow was already 2 times lower compared with the control model.

Introducing stenosis in the distal outflow section of both control and CERAB models caused a 2-fold decrease in flow velocity and a 3-fold drop in TAWSS values. Several studies have previously shown that areas with low TAWSS correspond to regions that may exhibit atherosclerotic lesions, leading to the belief that low TAWSS causes an increased risk of plaque formation.¹⁵⁻¹⁷ In the CERAB reconstruction, this means that low TAWSS due to a distal stenosis could increase the risk of new or progressive plaques and therefore may accelerate disease progression, with potential detrimental consequences for stent-graft patency.

In the outflow tract of the CERAB configuration, a 2-fold decrease in WSS was seen compared to the control model, independent of the presence or severity of a distal stenotic lesion. This indicates that the risk of accelerated

disease progression due to distal stenosis might well be greater in patients treated with a CERAB compared with untreated patients. Progression of atherosclerosis can lead to failure of the CERAB configuration, which may lead to acute limb ischemia. Besides the possible mid- to long-term effects, more acute modes of failure could be attributed to the fact that low WSS also increases the risk of thrombosis.¹⁸ Our group encountered early thrombosis in 2 patients 3 weeks after CERAB reconstructions.¹⁹

A previous study by Grimme et al¹ showed that outflow impairment near the CERAB configuration can cause occlusion of the stents and should therefore be monitored intensively and treated early.¹ The current study provides *in vitro* local hemodynamic data that suggest stenotic lesions more distal to the CERAB configuration could have the same effect. Treatment of this type of lesion, when significant, should therefore be considered in patients with a CERAB configuration, regardless of the patient's symptom status. In the case of nonsignificant stenosis, an increase in follow-up intensity should be considered. Placement of the stent configuration should likely be combined with femoral endarterectomy in patients with a preexisting stenotic lesion around the femoral bifurcation.²⁰

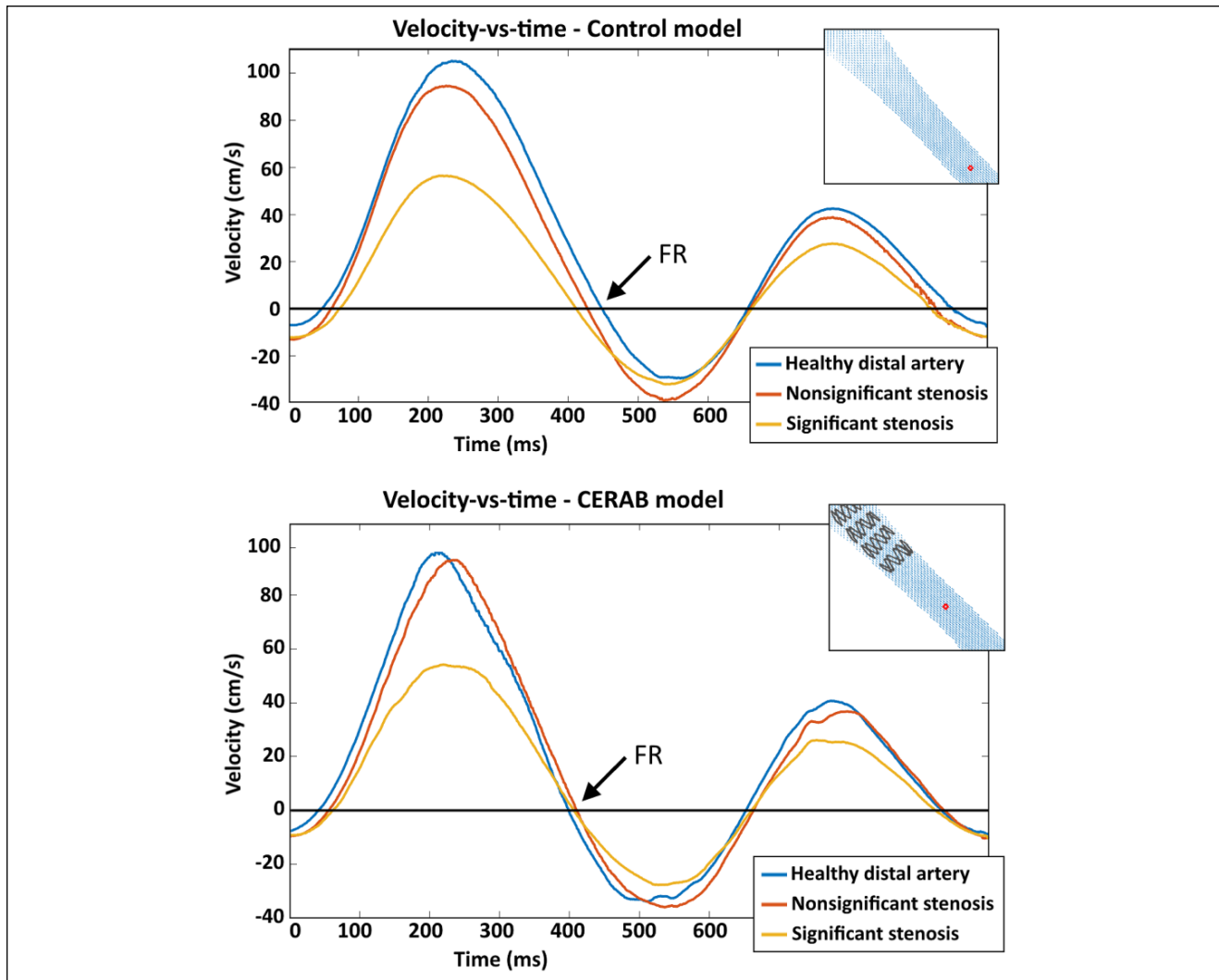


Figure 8. Velocity vs time plots of outflow region of interest in the control and covered endovascular reconstruction of the aortic bifurcation (CERAB) model. Locations of velocities are indicated by the red dots in the top right panels. FR, moment of flow reversal.

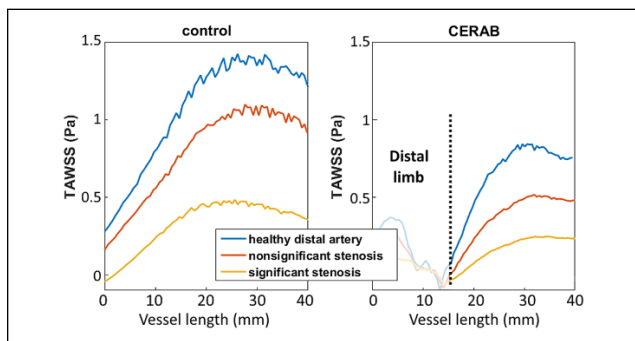


Figure 9. Time-averaged wall shear stress (TAWSS) in the outflow region of interest (left iliac artery, lateral wall) of the control model and covered endovascular reconstruction of the aortic bifurcation (CERAB) model. Length 0 is just distal of the bifurcation. The dashed line represents the distal edge of the left CERAB limb.

The lower WSS values in the outflow tract of the CERAB configuration seem to be related to the distal leg rather than the proximal cuff. This finding could also apply to other stent configurations that create a neobifurcation, such as kissing stents or grafts used for open surgery, as the extension of the iliac lumen gives rise to a more developed flow profile, with lower TAWSS values. A previous *in vitro* study by Walker et al²¹ also showed lower WSS downstream of a stent wire, lending credibility to this assumption. This would mean that treatment of stenosis distal to a stent should be considered in all patients, not only in patients with a CERAB configuration.

Besides WSS, the oscillatory nature of WSS, reported as the oscillatory shear index (OSI), also correlates with the progression and development of atherosclerosis.²² Higher OSI values indicate a balanced variation between the positive and negative directions of WSS. The metric was not

included in these results because the observed pattern depicted the inverse of the WSS curves. The PSV decreased (positive WSS) with increasing stenosis severity, balancing with the backflow (negative WSS) component and causing an increase in OSI.

Limitations

Several limitations inherent to in vitro studies influenced the results of this study, such as the compliance of the vessels, interaction between the stent and vascular endothelium, and movement of the vessels, which were not modeled in the in vitro setup. Stent covers made of transparent polyurethane were used to simulate the geometry of the CERAB for obtaining optical access. There was no attempt to mimic the material properties of expanded polytetrafluoroethylene. Furthermore, direct measurement of WSS using PIV techniques is not possible. Therefore, WSS values were always based on the velocity profile normal to the wall, which can be obtained only at a finite distance from the wall. This necessitates an interpolation of the flow profile to the wall, possibly introducing a measurement error. A high spatial and temporal resolution in combination with accurate wall detection is therefore needed to calculate the WSS with reasonable accuracy.

Lower WSS distal to the stents, such as observed in this in vitro study, may not be present in vivo, for example, due to the reorganization of endothelial cells around the stent edges and the compliance of arteries. Thus, in vivo studies to quantify blood flow patterns around stents are required. It should be noted, however, that in vivo flow quantification, with high spatial and temporal resolution, is not a simple matter. Aside from resolution constraints, magnetic resonance imaging–based techniques for in vivo flow quantification in stents create considerable material-dependent artifacts that may inhibit quantitative analysis near the stent configuration.²³ Contrast-enhanced, high-frame-rate, ultrasound-based techniques (echoPIV) could prove to be a convenient modality to quantify the in- and outflow of stent configurations. Until now, echoPIV techniques have been used only in superficial vessels and cardiac applications in a research setting.²⁴ Furthermore, clinical follow-up studies should be performed to investigate the effect of WSS on stent patency and subsequent clinical outcome.

Another relevant difference between the in vitro model and human physiology is the iliac outflow tract of the measurement setup. Both iliac vessels were connected to a single compliance and resistance. Therefore, during measurements, a decreased flow in the stenotic vessel automatically led to an increased flow in the contralateral vessel. In human physiology, the demand of oxygen is regulated for each organ individually by adjusting vascular resistance. Thus, in principle, a different redistribution of flow could take place. However, the redistribution of flow through the entire body

due to a stenosis in a single vessel is complex and was therefore not simulated in this study. Furthermore, a left-right comparison was not attempted. However, a future study accurately modeling the flow distribution would be of interest, and the addition of a contralateral stenosis would add further strength to the analysis.

Conclusion

This in vitro study shows that stenotic lesions distal to the aortic bifurcation cause a decrease in peak flow velocities and a corresponding decrease in TAWSS in the outflow tract of both the control and CERAB models. In the outflow tract of the CERAB configuration, TAWSS was lower than in the control independent of the severity of the distal stenotic lesion, indicating that local accelerated disease progression could be greater in patients treated with the CERAB technique. Therefore, treatment of stenotic lesions distal to a CERAB configuration could be indicated regardless of the presence or absence of symptoms. In vivo assessment of local flow patterns in combination with patient follow-up is required to verify these findings.

Authors' Note

Preliminary data were presented at the VEITH Symposium (November 15–19, 2016; New York, NY, USA).

Declaration of Conflicting Interests

The author(s) declared the following potential conflicts of interest with respect to the research, authorship, and/or publication of this article: Michel M. P. J. Reijnen has been paid a consulting fee by the Maquet Getinge Group and is on their speaker's bureau.

Funding

The author(s) received no financial support for the research, authorship, and/or publication of this article.

References

1. Grimme FA, Verbruggen PJ, Reijnen MM. The first results of the covered endovascular reconstruction of the aortic bifurcation (CERAB) technique for aortoiliac occlusive disease. *Eur J Vasc Endovasc Surg*. 2015;50:638–647.
2. Groot Jebbink E, Mathai V, Boersen JT, et al. Hemodynamic comparison of stent configurations used for aortoiliac occlusive disease. *J Vasc Surg*. 2017;66:251–260.e1.
3. Slager CJ, Wentzel JJ, Gijzen FJ, et al. The role of shear stress in the generation of rupture-prone vulnerable plaques. *Nat Clin Pract Cardiovasc Med*. 2005;2:401–407.
4. Clark TW, Groffsky JL, Soulen MC. Predictors of long-term patency after femoropopliteal angioplasty: results from the STAR registry. *J Vasc Interv Radiol*. 1994;12:923–933.
5. Ihnat DM, Duong ST, Taylor ZC, et al. Contemporary outcomes after superficial femoral artery angioplasty and stenting: The influence of TASC classification and runoff score. *J Vasc Surg*. 2008;47:967–974.

6. Yacyszyn VJ, Thatipelli MR, Lennon RJ, et al. Predictors of failure of endovascular therapy for peripheral arterial disease. *Angiology*. 2006;57:403–417.
7. Kavaliauskienė Ž, Benetis R, Inčiūra D, et al. Factors affecting primary patency of stenting for TransAtlantic Inter-Society (TASC II) type B, C, and D iliac occlusive disease. *Medicina*. 2014;50:287–294.
8. Groot Jebbink E, Goverde PC, van Oostayen JA, et al. Innovation in aortoiliac stenting: an in vitro comparison. *SPIE Med Imaging*. 2014;9036:90361X.
9. Groot Jebbink E, Grimme FA, Goverde PC, et al. Geometrical consequences of kissing stents and the Covered Endovascular Reconstruction of the Aortic Bifurcation configuration in an in vitro model for endovascular reconstruction of aortic bifurcation. *J Vasc Surg*. 2015;61:1306–1311.
10. Moore JE Jr, Ku DN, Zarins CK, et al. Pulsatile flow visualization in the abdominal aorta under differing physiologic conditions: implications for increased susceptibility to atherosclerosis. *J Biomech Eng*. 1992;114:391–397.
11. Garcia LA, Carrozza JP. Physiologic evaluation of translesion pressure gradients in peripheral arteries: comparison of pressure wire and catheter-derived measurements. *J Interv Cardiol*. 2007;20:63–65.
12. Gross CM, Krämer J, Weingärtner O, et al. Determination of renal arterial stenosis severity: comparison of pressure gradient and vessel diameter. *Radiology*. 2001;220:751–756.
13. Holenstein R, Ku DN. Reverse flow in the major infra-renal vessels—a capacitive phenomenon. *Biorheology*. 1988;25:835–842.
14. Leguy CA, Bosboom EM, Hoeks AP, et al. Model-based assessment of dynamic arterial blood volume flow from ultrasound measurements. *Med Biol Eng Comput*. 2009;47:641–648.
15. Frydrychowicz A, Stalder AF, Russe MF, et al. Three-dimensional analysis of segmental wall shear stress in the aorta by flow-sensitive four-dimensional-MRI. *J Magn Reson Imaging*. 2009;30:77–84.
16. Harloff A, Nußbaumer A, Bauer S, et al. In vivo assessment of wall shear stress in the atherosclerotic aorta using flow-sensitive 4D MRI. *Magn Reson Med*. 2010;63:1529–1536.
17. Markl M, Wegent F, Zech T, et al. In vivo wall shear stress distribution in the carotid artery: effect of bifurcation geometry, internal carotid artery stenosis, and recanalization therapy. *Circ Cardiovasc Imaging*. 2010;3:647–655.
18. Koskinas KC, Chatzizisis YS, Antoniadis AP, et al. Role of endothelial shear stress in stent restenosis and thrombosis. *J Am Coll Cardiol*. 2012;59:1337–1349.
19. Taeymans K, Groot Jebbink E, Holewijn S, et al. Midterm outcome of the Covered Endovascular Reconstruction of the Aortic Bifurcation (CERAB) technique for aortoiliac occlusive disease. *J Vasc Surg*. 2017 [in press].
20. Taurino M, Persiani F, Fantozzi C, et al. Trans-Atlantic Inter-Society Consensus II C and D iliac lesions can be treated by endovascular and hybrid approach: a single-center experience. *Vasc Endovasc Surg*. 2014;48:123–128.
21. Walker AM, Johnston CR, Rival DE. The quantification of hemodynamic parameters downstream of a Gianturco Zenith stent wire using Newtonian and non-Newtonian analog fluids in a pulsatile flow environment. *J Biomech Eng*. 2012;134:111001.
22. Ku DN, Giddens DP, Zarins CK, et al. Pulsatile flow and atherosclerosis in the human carotid bifurcation. Positive correlation between plaque location and low oscillating shear stress. *Arteriosclerosis*. 1985;5:293–302.
23. Bunck AC, Juttner A, Kroger JR, et al. 4D phase contrast flow imaging for in-stent flow visualization and assessment of stent patency in peripheral vascular stents—a phantom study. *Eur J Radiol*. 2012;81:E929–E937.
24. Poelma C. Ultrasound imaging velocimetry: a review. *Exp Fluids*. 2017;58:3. doi:10.1007/s00348-016-2283-9.